

# Visualising crystal packing interactions in solid-state NMR: Concepts and applications

EP

Cite as: J. Chem. Phys. **147**, 144203 (2017); <https://doi.org/10.1063/1.4996750>

Submitted: 18 July 2017 . Accepted: 12 September 2017 . Published Online: 11 October 2017

Miri Zilka , Simone Sturniolo , Steven P. Brown , and Jonathan R. Yates 

## COLLECTIONS

EP This paper was selected as an Editor's Pick



View Online



Export Citation



CrossMark

## ARTICLES YOU MAY BE INTERESTED IN

[Robust determination of the chemical potential in the pole expansion and selected inversion method for solving Kohn-Sham density functional theory](#)

The Journal of Chemical Physics **147**, 144107 (2017); <https://doi.org/10.1063/1.5000255>

[Resonant-convergent second-order nonlinear response functions at the levels of Hartree-Fock and Kohn-Sham density functional theory](#)

The Journal of Chemical Physics **147**, 144109 (2017); <https://doi.org/10.1063/1.4991616>

[Effective Floquet Hamiltonian theory of multiple-quantum NMR in anisotropic solids involving quadrupolar spins: Challenges and Perspectives](#)

The Journal of Chemical Physics **147**, 144202 (2017); <https://doi.org/10.1063/1.4993313>

PHYSICS TODAY  
WHITEPAPERS

### ADVANCED LIGHT CURE ADHESIVES

Take a closer look at what these environmentally friendly adhesive systems can do

READ NOW

PRESENTED BY  
**MASTERBOND**  
ADHESIVES | SEALANTS | COATINGS

# Visualising crystal packing interactions in solid-state NMR: Concepts and applications

Miri Zilka,<sup>1</sup> Simone Sturniolo,<sup>2</sup> Steven P. Brown,<sup>1,a)</sup> and Jonathan R. Yates<sup>3,b)</sup>

<sup>1</sup>*Department of Physics, University of Warwick, Coventry CV4 7AL, United Kingdom*

<sup>2</sup>*Scientific Computing Department, Rutherford Appleton Laboratory, Chilton, Didcot, Oxfordshire OX11 0QX, United Kingdom*

<sup>3</sup>*Department of Materials, University of Oxford, Oxford OX1 3PH, United Kingdom*

(Received 18 July 2017; accepted 12 September 2017; published online 11 October 2017)

In this article, we introduce and apply a methodology, based on density functional theory and the gauge-including projector augmented wave approach, to explore the effects of packing interactions on solid-state nuclear magnetic resonance (NMR) parameters. A visual map derived from a so-termed “magnetic shielding contribution field” can be made of the contributions to the magnetic shielding of a specific site—partitioning the chemical shift to specific interactions. The relation to the established approaches of examining the molecule to crystal change in the chemical shift and the nuclear independent chemical shift is established. The results are applied to a large sample of 71 molecular crystals and three further specific examples from supermolecular chemistry and pharmaceuticals. This approach extends the NMR crystallography toolkit and provides insight into the development of both cluster based approaches to the predictions of chemical shifts and for empirical predictions of chemical shifts in solids. © 2017 Author(s). All article content, except where otherwise noted, is licensed under a Creative Commons Attribution (CC BY) license (<http://creativecommons.org/licenses/by/4.0/>). <https://doi.org/10.1063/1.4996750>

## I. INTRODUCTION

The magnetic shielding in nuclear magnetic resonance (NMR) experiments gives crucial information about the local structure of an atom of interest. Significant advances in solid-state NMR have generated a powerful tool for structural investigation. Combined with Powder X-Ray Diffraction (PXRD), the field of “NMR crystallography”<sup>1,2</sup> is gaining popularity as a structure determination strategy. Combining the two methods efficiently has been aided by the development of density functional theory (DFT) calculations, first in molecular systems<sup>3</sup> and more recently in crystalline solids, for example, the gauge-including projector augmented wave (GIPAW) approach.<sup>4,5</sup> Recent work has shown that the positional uncertainty in structures obtained by chemical-shift-based NMR crystallography can be significantly lower than that of single-crystal X-ray-diffraction-based structure determination.<sup>6</sup> “NMR crystallography” can also be applied to materials that are not perfectly crystalline, for example, semicrystalline polymers.<sup>7</sup> The role of first principle methods is often to simply predict or assign an experimental NMR spectrum, but they have the potential to do much more than this. We should look into such calculations to provide information on the origin of the NMR parameters—addressing the questions of why a particular species has a certain chemical shift and what this can tell us about its bonding environment.

Focusing on molecular crystals, several approaches have been employed to address these issues. For example, the molecule to crystal change in the chemical shift<sup>8–11</sup> compares the magnetic shielding calculated for a molecule in the full packed crystal structure to that for the same molecule in an isolated environment. This quantity highlights the contributions to the shielding in the solid state arising from combined effects of intermolecular interactions such as hydrogen bonding and long-range electrostatic effects such as the influence of ring currents in neighbouring molecules. To isolate the effects of ring currents, the Nucleus Independent Chemical Shift (NICS)<sup>12,13</sup> has been employed.<sup>14–17</sup>

In this work, we show how the magnetic shielding in solids can be broken down into contributions arising from different locations within the crystal: short-range contributions arising from currents close to the atom in question and contributions from long-range currents, away from the atom. We demonstrate how this long-range component can be visualised, highlighting the functional groups responsible for the magnetic shielding of a particular atom. We examine the relationship between this spatial decomposition of the origin of shielding and both the molecule to crystal change in the chemical shift and the NICS.

## II. METHODOLOGY

### A. Magnetic shielding

In a diamagnetic insulator, the magnetic shielding effect arises from the electronic current,  $\mathbf{j}(\mathbf{r})$ , induced by an applied magnetic field  $\mathbf{B}_{\text{ext}}$ . At a given point in space,  $\mathbf{r}$ , it is

<sup>a)</sup>Electronic mail: [s.p.brown@warwick.ac.uk](mailto:s.p.brown@warwick.ac.uk)

<sup>b)</sup>Electronic mail: [jonathan.yates@materials.ox.ac.uk](mailto:jonathan.yates@materials.ox.ac.uk)

characterized by the magnetic shielding tensor,  $\vec{\sigma}(\mathbf{r})$ , defined as the ratio between the locally induced field,  $\mathbf{B}_{\text{in}}(\mathbf{r})$ , and the applied field. This can be obtained from the current using the Biot-Savart law

$$\mathbf{B}_{\text{in}}(\mathbf{r}) = -\vec{\sigma}(\mathbf{r})\mathbf{B}_{\text{ext}} = \frac{1}{c} \int d^3r' \mathbf{j}(\mathbf{r}') \times \frac{\mathbf{r} - \mathbf{r}'}{|\mathbf{r} - \mathbf{r}'|^3}. \quad (1)$$

For  $\mathbf{r} = \mathbf{R}_i$ , i.e., the position of the  $i$ -th nucleus, then  $\vec{\sigma}(\mathbf{R}_i)$  is the magnetic shielding tensor of that nucleus. The isotropic magnetic shielding,  $\sigma(\mathbf{R}_i)$ , is given by  $\sigma(\mathbf{R}_i) = \text{Tr}[\vec{\sigma}(\mathbf{R}_i)]/3$ . It is important to note that the experimentally relevant parameter is the chemical shift. The isotropic chemical shift,  $\delta(\mathbf{R}_i)$ , is related to the isotropic magnetic shielding by

$$\delta(\mathbf{R}_i) = \frac{\sigma^{\text{ref}} - \sigma(\mathbf{R}_i)}{1 - \sigma(\mathbf{R}_i)}, \quad (2)$$

where  $\sigma^{\text{ref}}$  is the magnetic shielding of a nucleus of the same species in a chosen reference compound. For light elements,  $\sigma(\mathbf{R}_i) \ll 1$  and so

$$\delta(\mathbf{R}_i) = \sigma^{\text{ref}} - \sigma(\mathbf{R}_i). \quad (3)$$

Given the simple relation between the chemical shift and magnetic shielding, it is appropriate to focus on the interpretation of the latter quantity, noting that only differences in the magnetic shielding between the compound of interest and the reference compound can contribute to the observed chemical shift. In order to link the computed magnetic shielding to the underlying atomistic structure, it is natural to look for ways to partition the induced current and hence the magnetic shielding. There are many possible ways to do this, but it should be stressed that any such decomposition is for the purpose of interpretation as only the total magnetic shielding is an observable quantity. Some forms of decomposition are more suited to a given computational technique, for example, it is natural to divide the shielding into contributions from orbitals when working with a local-orbital quantum chemistry code, but such a decomposition is challenging in a planewave basis set, solid-state code. Here we focus on partitioning schemes that are particularly suited to the interpretation of the NMR parameters of molecular crystals working within a planewave-pseudopotential formalism.

## B. Local partitioning of current

We compute the induced current and hence the magnetic shielding using the planewave pseudopotential implementation of DFT, in particular using the GIPAW approach.<sup>18</sup> This provides a natural route to break down the magnetic shielding into contributions arising from short-range and long-range currents. Short-range is defined within this context as the current arising in the spherical region around the atom used for the PAW augmentation. The radius used for each element is given in Table I. The long-range contribution,  $\sigma^{\text{lr}}$ , is simply the contribution from currents outside of this sphere. The short-range, or local, contribution can be further divided into a diamagnetic,  $\sigma_{\text{dia}}^{\text{loc}}$ , and a paramagnetic contribution,  $\sigma_{\text{para}}^{\text{loc}}$  (paramagnetic contributions decrease the magnetic shielding, while diamagnetic ones increase it). We note that in general it is not possible to divide the total current in an extended solid (i.e., in a

TABLE I. Atomic radius and maximal variation of local and non-local as well as total GIPAW calculated magnetic shielding components (in ppm) for 71 molecular crystals.

	Radius (a.u.)	Local			$\sigma^{\text{lr}}$	$\sigma_{\text{tot}}$
		$\sigma_{\text{core}}^{\text{loc}}$	$\sigma_{\text{dia}}^{\text{loc}}$	$\sigma_{\text{para}}^{\text{loc}}$		
H	0.6	...	3.0	0.0	19.3	22.0
C	1.4	0.0	5.1	175.0	20.1	190.3
N	1.1	0.0	3.4	300.0	25.4	325.8
O	1.1	0.0	1.3	602.3	19.8	622.0

crystal) into diamagnetic and paramagnetic terms.<sup>19,20</sup> However, a localised current can be so divided—see Ref. 21 for a further discussion. Note that in a pseudopotential approach, the contribution of the core electrons to the shielding,  $\sigma_{\text{core}}$ , is computed in a free-atom calculation and therefore does not depend on the chemical environment—this has been shown to be an excellent approximation.<sup>22</sup> The total magnetic shielding can thus be written as

$$\sigma_{\text{tot}} = \sigma_{\text{core}} + \sigma_{\text{dia}}^{\text{loc}} + \sigma_{\text{para}}^{\text{loc}} + \sigma^{\text{lr}}. \quad (4)$$

The technical details of the implementation of this approach are given in the [supplementary material](#). We note that a similar decomposition has been presented for the electric field gradient in solids.<sup>23</sup>

## C. Molecule to crystal change in magnetic shielding and NICS

The molecule to crystal change in magnetic shielding,  $\Delta\sigma$ ,<sup>8–11</sup> is defined as the difference between the calculated shielding of a site in the full crystal and that for an isolated molecule (usually taken from the full crystal without change in the geometry),

$$\Delta\sigma = \sigma_{\text{crys}} - \sigma_{\text{mol}}. \quad (5)$$

The molecule to crystal shift can be computed for each of the terms in Eq. (4), giving, for example,  $\Delta\sigma^{\text{lr}}$  or  $\Delta\sigma_{\text{tot}}$ . It must be stressed that Eq. (5) reports the change in shielding. Previous papers have presented the change in the chemical shift,<sup>8–11</sup> i.e.,  $\Delta\delta$ , which is simply the negative of  $\Delta\sigma$ —see Eq. (3).  $\Delta\sigma$  can be considered to arise from two contributions: long-range effects of current elements, e.g., ring currents, and local changes in the electronic structure which take place upon crystal packing, e.g., hydrogen bonding. To quantify the long-range effects of current elements in the solid state, it is common to calculate the NICS,  $\sigma_{\text{NICS}}$ .<sup>10,11,16</sup> This can be computed directly from the current following Eq. (1). Again, for consistency, we emphasize that the NICS reported in this work refers to the shielding. One can compute the NICS using different models, for example, from a single isolated molecule or a plane of molecules.<sup>10</sup> For the purposes of interpreting long-range effects, we compute the NICS using a supercell approach which captures the effect of the nearest neighbour molecules.

The necessary calculations to compute the molecule to crystal change in magnetic shielding and the NICS are illustrated in Fig. 1. The first calculation,  $I_{\text{fullcell}}$ , is of a single,

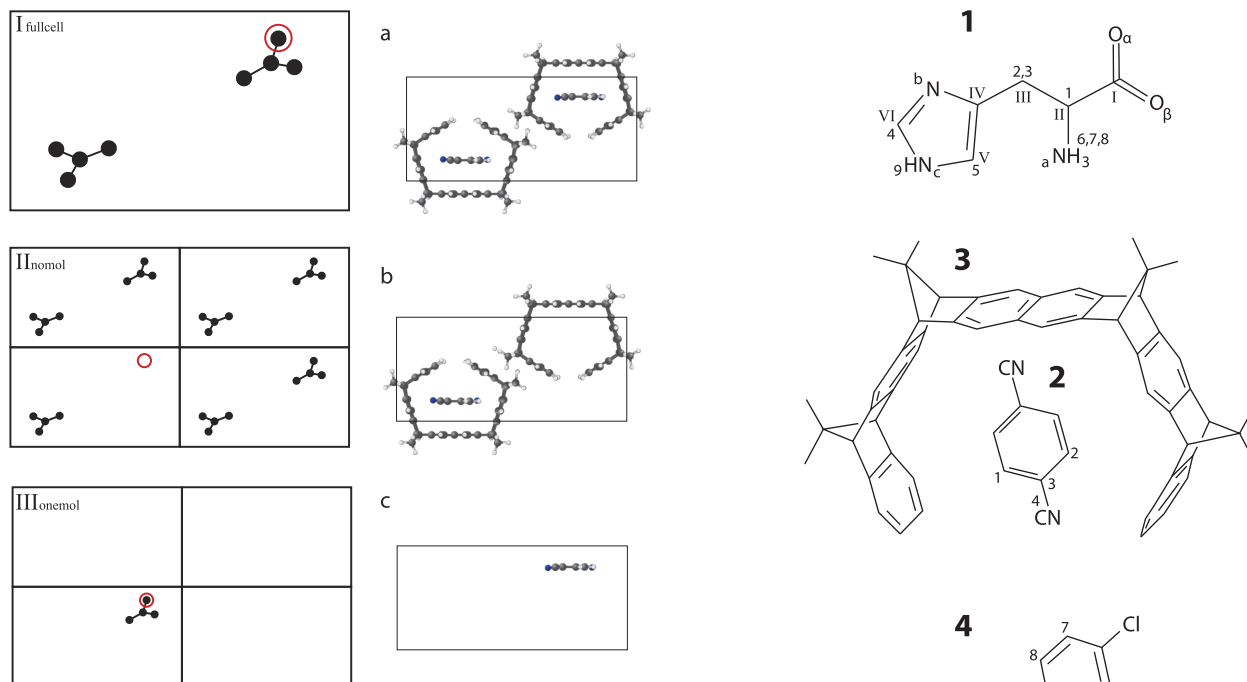


FIG. 1. Schematic illustration of the calculations required to decompose the non-local magnetic shielding components into distinct contributions. Left-hand side:  $I_{\text{fullcell}}$ ,  $II_{\text{nomol}}$ , and  $III_{\text{onemol}}$  represent the three required calculations. The red circle notes the position in space of the atom of interest. The first calculation,  $I_{\text{fullcell}}$ , is of a single, unaltered full crystallographic unit cell. The second one,  $II_{\text{nomol}}$ , is a cell with the molecule that the atom of interest belongs to removed. The shielding is calculated at the location of the specified atom. It may be necessary to simulate a larger supercell to ensure that the first nearest neighbours of the absent molecule are included.  $III_{\text{onemol}}$ : A supercell containing only the molecule with the atom of interest. Right hand side: an illustration of the three calculations for **2:3**.

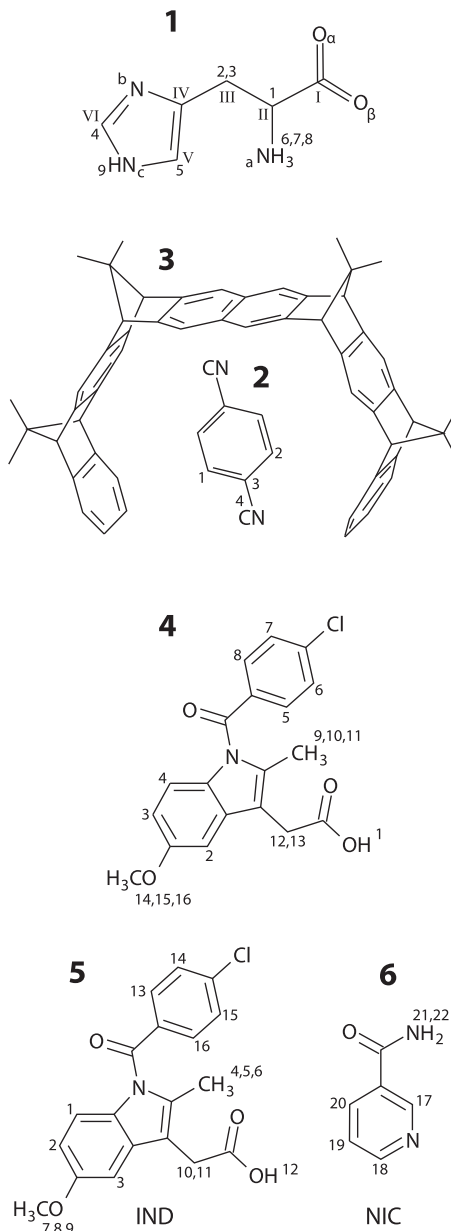
unaltered full crystallographic unit cell. The second calculation,  $II_{\text{nomol}}$ , is for a cell of the crystal with the molecule which contains the atom of interest removed. Depending on the crystal structure, it may be necessary to simulate a supercell of the unit cell, such that the missing molecule is surrounded by all of its nearest neighbours. The final calculation,  $III_{\text{onemol}}$ , is a vacuum supercell with only the molecule containing the atom of interest. The NICS,  $\sigma_{\text{NICS}}$ , is obtained from the calculation on  $II_{\text{nomol}}$  as the value of the magnetic shielding at the site of the atom in the missing molecule. The molecule to crystal change in magnetic shielding,  $\Delta\sigma$ , is the change in the shielding between calculations  $III_{\text{onemol}}$  and  $I_{\text{fullcell}}$ , i.e.,  $\Delta\sigma = \sigma(I_{\text{fullcell}}) - \sigma(III_{\text{onemol}})$ .

#### D. Magnetic shielding contribution field

To further analyze the origin of the non-local contribution to the magnetic shielding, we consider a tensor field,  $\vec{G}_{\mathbf{R}_i}(\mathbf{r})$ , which we call the Magnetic Shielding Contribution Field (MSCF). This represents the contribution to the magnetic shielding of the  $i$ -th nucleus from the induced current at the point  $\mathbf{r}$ ,

$$-\vec{G}_{\mathbf{R}_i}(\mathbf{r})\mathbf{B}_{\text{ext}} = \frac{1}{c}\mathbf{j}(\mathbf{r}') \times \frac{\mathbf{r} - \mathbf{r}'}{|\mathbf{r} - \mathbf{r}'|^3}. \quad (6)$$

Following Eq. (1), the magnetic shielding is given as the integral of the MSCF over all space



SCHEME 1.

$$\vec{\sigma}(\mathbf{R}_i) = \int \vec{G}_{\mathbf{R}_i}(\mathbf{r}) d^3r. \quad (7)$$

To aid the interpretation of the isotropic magnetic shielding, it is useful to introduce the isotropic MSCF,  $G_{\mathbf{R}_i}(\mathbf{r})$ , given by

$$G_{\mathbf{R}_i}(\mathbf{r}) = \frac{1}{3} \text{Tr} [\vec{G}_{\mathbf{R}_i}(\mathbf{r})]. \quad (8)$$

The MSCF can be computed for the geometries outlined in Sec. II C. The MSCF computed for  $I_{\text{fullcell}}$  provides a visualization of  $\sigma^{\text{lr}}$  while that for  $II_{\text{nomol}}$  is a visualization of  $\sigma_{\text{NICS}}$ . We note that in Ref. 24, the MSCF is mapped onto an isosurface of the current density in order to examine intermolecular interactions.

#### E. Calculation details

In order to provide insight as to the origin of the magnetic shielding in molecular crystals, we require a set of systems

which span a wide range of possible chemical environments. For the statistical analysis, we include 71 molecular crystals; 54 are taken from a set whose structures were recently re-determined with refined proton positions in Ref. 25 and 17 are amino acids with starting structures as from the recommendations in Ref. 26. For a more detailed analysis, we focus on a number of compounds (see Scheme 1, numbering in each case follows that in the CASTEP generated magres file) that have been previously examined in the context of significant solid-state effects on NMR chemical shifts.<sup>27–30</sup>

All calculations used a developer version of the CASTEP code<sup>31</sup> together with the CASTEP9 set of ultrasoft pseudopotentials.<sup>32</sup> The cutoff for the basis set was 800 eV and the Brillouin zone was sampled using a Monkhorst-Pack<sup>33</sup> grid with a minimum spacing of  $0.05 \times 2\pi \text{ \AA}^{-1}$ . All crystal structures were optimized using the PBE<sup>34</sup> functional together with dispersion corrections using the Tkatchenko-Scheffler (TS) scheme.<sup>35</sup> Both unit cell parameters and internal coordinates were able to relax during the optimization. Calculations of NMR magnetic shieldings were computed using the GIPAW approach.<sup>18,36</sup> The relaxed crystal structures and full shielding tensors for all atoms are made available as a downloadable data set.

### III. RESULTS

#### A. Partitioning of the magnetic shielding

We consider the partitioning of the magnetic shielding into contributions from local and long-range currents following Eq. (4). We first focus on the specific example of L-histidine, **1**, reported in Table II. For  $^1\text{H}$ , the variation in the magnetic shielding can be seen to arise predominantly from  $\sigma^{lr}$ , i.e., from currents located away from the atom. The local contribution for  $^1\text{H}$  is purely diamagnetic. This is because a paramagnetic contribution requires the wavefunction close to the nucleus to have at least “p” character. This diamagnetic contribution can be seen to show only a small variation with respect to the chemical environment. For  $^{13}\text{C}$ ,  $\sigma^{lr}$  gives a proportionally smaller contribution to the total variation in magnetic shielding.  $\sigma_{dia}^{loc}$  again exhibits only a small dependence on the chemical environment; however,  $\sigma_{para}^{loc}$  is large and dominates the variation in the total magnetic shielding.

Figure 2 shows a histogram of the four contributions to the magnetic shielding in Eq. (4) for a full set of 71 molecular crystals. The variation in each term, i.e., the contribution to the chemical shift, is summarized in Table I. From this, it is evident that the contribution of the non-local currents to the chemical shift is almost independent of species, and it is the increase in the local paramagnetic contribution which is responsible for the much larger chemical shift range of the heavier elements. For oxygen, the non-local term contributes only 3% to the chemical shift variation while for hydrogen it is 87%. This picture is not unexpected: The contribution of an element of current to the magnetic shielding at a particular nucleus depends only on the distance of the nucleus from the current element and not on the type of nucleus. As an illustration, consider the ring current effect from an aromatic group. The shielding induced by this ring on a close by atom depends

TABLE II. Local vs non-local decomposition of the GIPAW calculated magnetic shielding (in ppm) for L-histidine. See Scheme 1 for atom labels.

	Label	$\sigma_{core}^{loc}$	$\sigma_{dia}^{loc}$	$\sigma_{para}^{loc}$	$\sigma^{lr}$	$\sigma_{tot}$
H	1	0.0	9.4	0.0	17.4	26.8
	2	0.0	9.2	0.0	19.0	28.3
	3	0.0	9.2	0.0	18.9	28.1
	4	0.0	9.2	0.0	15.5	24.7
	5	0.0	9.2	0.0	16.7	25.8
	6	0.0	8.2	0.0	13.1	21.3
	7	0.0	8.3	0.0	12.1	20.4
	8	0.0	8.2	0.0	12.4	20.6
	9	0.0	8.0	0.0	6.9	14.9
C	$\Delta \max^a$	...	1.3	...	12.1	13.4
	$\mu^b$	0.0	8.8	0.0	14.7	23.4
	$\sigma^c$	...	0.5	...	3.7	4.2
	I	200.5	47.4	−263.3	8.7	−6.8
	II	200.5	47.4	−149.4	16.7	115.1
	III	200.5	48.3	−122.4	20.1	146.5
	IV	200.5	48.4	−236.4	19.0	31.5
	V	200.5	48.7	−230.5	19.0	37.7
	VI	200.5	48.8	−213.8	21.4	56.9
	$\Delta \max^a$	...	1.4	141.0	12.7	153.3
	$\mu^b$	200.5	48.2	−202.6	17.5	63.5
	$\sigma^c$	...	0.6	50.0	4.2	52.0
N	a	235.8	62.4	−148.9	37.2	186.5
	b	235.8	61.3	−355.3	30.9	−27.4
	c	235.8	62.2	−285.8	33.3	45.4
	$\Delta \max^a$	...	1.1	206.4	6.3	213.9
O	$\mu^b$	235.8	62.0	−263.4	33.8	68.2
	$\sigma^c$	...	0.5	85.7	2.6	88.8
	$\alpha$	271.1	95.8	−431.1	31.9	−32.3
	$\beta$	271.1	95.8	−436.4	31.9	−37.7
	$\Delta \max^a$	...	...	5.3	0.0	5.4
	$\mu^b$	271.1	95.8	−433.8	31.9	−35.0
	$\sigma^c$	...	...	2.7		2.7

<sup>a</sup>The maximal difference.

<sup>b</sup>Mean.

<sup>c</sup>Standard deviation.

only on the distance of the atom from the ring and not on the species of the atom. So the long-range effects of currents should be similar for all atom types. The observed effect on  $^1\text{H}$  is simply greater due to the absence of a significant on-site contribution. In addition, the effect on  $^1\text{H}$  is also enhanced as hydrogen atoms are more likely to be found in closer proximity to neighbouring functional groups.

#### B. Ring currents and MSCF

A common approach to understanding the packing effects on NMR parameters is to look at the changes in magnetic shielding between a molecule in the full packed crystal structure and the same molecule in an isolated environment—corresponding to the so-called molecule to crystal change in the chemical shift.<sup>8–11</sup> We now focus on three systems that have been previously studied in this way.<sup>27–30</sup> Focusing first on a host-guest molecular tweezer,<sup>27,28</sup> we look at the local and



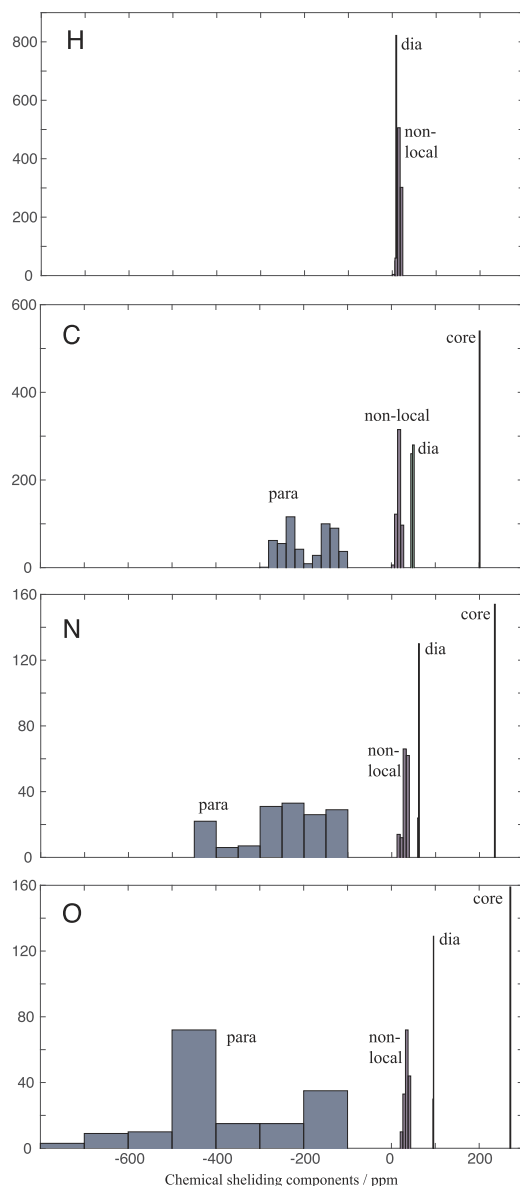


FIG. 2. Histogram of the different components contributing to the GIPAW calculated H, C, N, and O magnetic shielding for 71 molecular crystals. The three local components, i.e., from within the atomic sphere: core, diamagnetic, and paramagnetic, and the non-local contribution are plotted.

non-local contributions to  $\Delta\sigma$  for the guest 1,4-dicyanobenzene molecule (**2**). Table III shows that for  $^1\text{H}$ , the total  $\Delta\sigma_{\text{tot}}$  is almost entirely (to within 0.15 ppm) due to the long-range currents and  $\Delta\sigma_{\text{lr}}$  is in close agreement with  $\sigma_{\text{NICS}}$ . This is reasonable as the packing effects are expected to be due to the presence of ring currents in the host “tweezer” compound.<sup>27,28</sup> By plotting the isotropic MSCF  $G_R(r)$ , from Eq. (8), in Fig. 3, we can highlight the regions of space that give rise to this non-local contribution for a given atom. Figure S1 in the [supplementary material](#) presents the separate positive and negative contributions. Atom H2 has a larger  $\sigma_{\text{NICS}}$  than H1 (5.76 ppm vs 2.52 ppm). Figure 3 shows that H2 is aligned centrally to the neighbouring ring and has a strong contribution from that ring as well as the neighbouring ring. In contrast, H1 is aligned off-center from its nearest ring with a correspondingly smaller contribution from that ring.

TABLE III. GIPAW calculated  $^1\text{H}$  and  $^{13}\text{C}$  magnetic shielding contributions (in ppm) for 1,4-dicyanobenzene **2** in the **2:3** molecular tweezer. The nucleus under consideration is shown in bold.

	Group	Label	$\sigma_{\text{dia}}^{\text{loc}}$	$\sigma_{\text{para}}^{\text{loc}}$	$\sigma_{\text{lr}}$	$\sigma_{\text{tot}}^{\text{a}}$	$\sigma_{\text{NICS}}$
Isolated molecule	<b>CH</b>	1	9.09	0.00	12.54	21.63	
	<b>CH</b>	2	9.25	0.00	13.55	22.80	
	<b>CH</b>	1	48.87	−233.44	17.84	33.78	
	<b>CH</b>	2	48.88	−231.46	17.84	35.76	
	<b>CH</b>	3	48.77	−211.93	17.84	55.19	
	<b>CH</b>	4	50.70	−221.86	17.87	47.22	
Full crystal	<b>CH</b>	1	9.12	0.00	15.05	24.17	
	<b>CH</b>	2	9.21	0.00	19.19	28.40	
	<b>CH</b>	1	48.86	−232.96	21.27	37.68	
	<b>CH</b>	2	48.90	−233.56	22.58	38.43	
	<b>CH</b>	3	48.79	−210.91	21.46	59.85	
	<b>CH</b>	4	50.60	−224.23	19.60	46.49	
$\Delta\sigma$	<b>CH</b>	1	0.03	0.00	2.51	2.54	2.52
	<b>CH</b>	2	−0.04	0.00	5.63	5.59	5.76
	<b>CH</b>	1	−0.01	0.49	3.42	3.90	3.59
	<b>CH</b>	2	−0.02	2.10	4.74	2.66	4.67
	<b>CH</b>	3	0.02	1.02	3.62	4.66	3.53
	<b>CH</b>	4	−0.09	−2.37	1.73	−0.74	2.02

<sup>a</sup>For  $^{13}\text{C}$ ,  $\sigma_{\text{tot}}$  includes the  $\sigma_{\text{core}}^{\text{loc}}$  contributions of 200.51 ppm.

For  $^{13}\text{C}$ , the situation is more complicated. Table III shows that  $\Delta\sigma_{\text{tot}}$  is not well correlated to  $\sigma_{\text{NICS}}$ . From the non-local decomposition, we see that in fact  $\sigma_{\text{NICS}}$  closely matches the non-local ( $\sigma_{\text{lr}}$ ) contribution to  $\Delta\sigma_{\text{tot}}$ ; however, there is a significant change in the local contribution to the shielding. Depending on the site in question, this can either increase or decrease  $\Delta\sigma_{\text{tot}}$ . This local contribution arises from changes in the current close to the C nucleus due to the effects of the packing environment. It is therefore not straightforward to interpret  $\Delta\sigma_{\text{tot}}$  of 2nd period elements in terms of long-range effects such as ring currents, and the decomposition into short- and long-range current contributions assists with the interpretation.

### C. Hydrogen bonding

As an example of hydrogen bonded compounds, we consider both the  $\gamma$  polymorph of indomethacin<sup>29</sup> and a co-crystal of indomethacin and nicotinamide (IND-NIC).<sup>30</sup> The decomposition of the  $^1\text{H}$  shielding for  $\gamma$ -indomethacin, and the indomethacin and nicotinamide molecules in the co-crystal is reported in Tables IV–VI, respectively. The decomposition of the shielding for the remaining elements in these compounds is reported in the [supplementary material](#). We find that again it is the changes in the non-local term which contribute to the majority of the variation in the chemical shift. The maximum change in the local contribution is <0.4 ppm; however, it is typically much smaller than this. In the absence of any hydrogen bonding, we see close agreement between  $\sigma_{\text{NICS}}$  and the contribution of  $\sigma_{\text{lr}}$  to the molecule to crystal change in the chemical shift. For example, atom H7 of IND in IND-NIC (see Table V) (**5**) is located just above an aromatic ring in the neighbouring molecule—and has no oxygen atom available

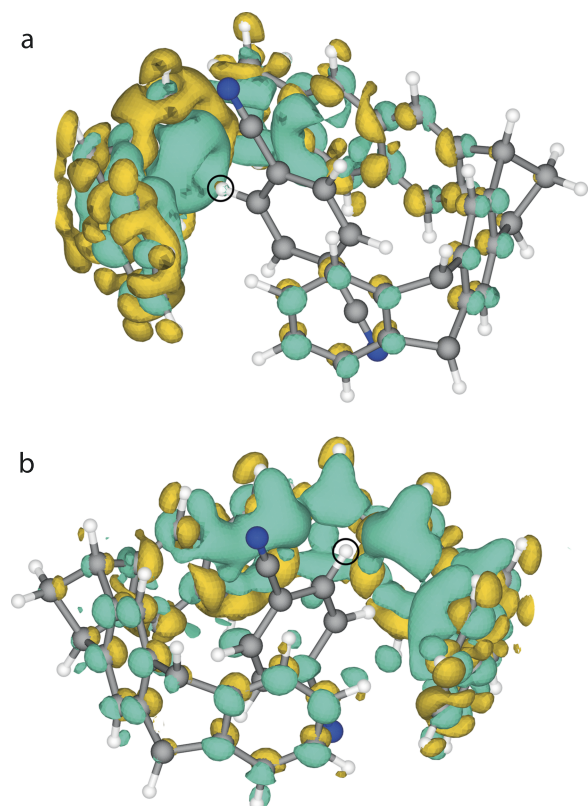


FIG. 3. Magnetic Shielding Contribution Field (MSCF) for two proton sites in 1,4-dicyanobenzene (**2**) with a naphthalene-spaced tweezer **2:3** as obtained from the  $II_{\text{nomol}}$  calculation (see Fig. 1). (a) shows the MSCF for site H2 and (b) for site H1. In both cases, the atom under consideration is highlighted with a black circle. The calculation has been performed with the  $II_{\text{nomol}}$  cell, thus showing the contribution from the naphthalene-spaced tweezer. The magnitude and sign of  $G_R$  [Eq. (8)] are plotted as an isosurface containing volume elements that contribute 0.000 25 ppm or more for (a) and 0.000 18 ppm for (b) to the shielding of the hydrogen (element volume  $0.0019 \text{ \AA}^3$ ). Yellow elements increase the  $\sigma_{\text{NICS}}$  value and turquoise elements decrease the  $\sigma_{\text{NICS}}$  value.

for hydrogen bonding within  $3 \text{ \AA}$ . H7 has  $\Delta\sigma_{\text{tot}} = 2.36 \text{ ppm}$  in close agreement with the NICS value,  $\sigma_{\text{NICS}} = 2.54 \text{ ppm}$ . However, it should not be assumed that a large  $\sigma_{\text{NICS}}$  is due to the presence of a ring current. Consider the case of H18 in NIC (**6**) shown in Table VI. For this site,  $\Delta\sigma_{\text{tot}} = -1.53 \text{ ppm}$  and  $\Delta\sigma_{\text{lr}} = -1.43 \text{ ppm}$  are both in close agreement with the NICS value,  $\sigma_{\text{NICS}} = -1.30 \text{ ppm}$ . Note that here  $\sigma_{\text{NICS}}$  is of the opposite sign to the value observed for an atom located above an aromatic ring (see Sec. III B). Examining the MSCF in Fig. 4 shows a significant contribution from currents around an oxygen atom located at a distance of  $2.7 \text{ \AA}$  to the long range contribution to the shielding. This distance is at the upper limit to what has been regarded as a weak ( $\text{CH} \cdots \text{O}$ ) hydrogen bond.<sup>8</sup> At shorter weak hydrogen bond distances, we find that there is a marked long-range contribution to  $\Delta\sigma$  which is not reflected in  $\sigma_{\text{NICS}}$ , e.g., in Table VI, atom H17 has  $\Delta\sigma_{\text{lr}} = -1.07 \text{ ppm}$  and  $\sigma_{\text{NICS}} = 0.02 \text{ ppm}$ . The effect is more pronounced for strongly hydrogen bonded protons, e.g.,  $\Delta\sigma_{\text{lr}} = -6.83 \text{ ppm}$  and  $\sigma_{\text{NICS}} = 0.35 \text{ ppm}$ , for OH (H1) in  $\gamma$ -IND (**4**) (see Table IV).

In order to understand more clearly the origin of this non-local component, in Fig. 5, we show plots of the isotropic

TABLE IV. GIPAW calculated  $^1\text{H}$  magnetic shielding (in ppm) for  $\gamma$ -IND (**4**).<sup>a</sup>

	Group	Label	$\sigma_{\text{dia}}^{\text{loc}}$	$\sigma_{\text{lr}}$	$\sigma_{\text{tot}}$	$\sigma_{\text{NICS}}$	$r_{\text{H}\cdots\text{O}}(\text{\AA})^b$
Isolated molecule	OH	1	7.94	15.39	23.33		
	CH	6	9.24	14.65	23.89		
	CH <sub>2</sub>	12	9.11	18.24	27.35		
	CH <sub>2</sub>	13	9.25	17.78	27.04		
	H <sub>3</sub> CO	14	9.35	17.97	27.32		
	H <sub>3</sub> CO	16	9.40	17.53	26.93		
Full crystal	OH	1	7.58	8.56	16.14		
	CH	6	9.23	15.65	24.87		
	CH <sub>2</sub>	12	9.07	20.09	29.16		
	CH <sub>2</sub>	13	9.22	19.70	28.92		
	H <sub>3</sub> CO	14	9.30	20.30	29.59		
	H <sub>3</sub> CO	16	9.33	18.15	27.48		
$\Delta\sigma$	OH	1	-0.36	-6.83	-7.19	0.35	1.64
	CH	6	-0.02	1.00	0.98	1.11	2.99
	CH <sub>2</sub>	12	-0.04	1.85	1.81	1.71	...
	CH <sub>2</sub>	13	-0.03	1.91	1.88	1.67	...
	H <sub>3</sub> CO	14	-0.05	2.33	2.28	2.41	...
	H <sub>3</sub> CO	16	-0.07	0.62	0.55	1.19	2.63

<sup>a</sup>Only protons with either  $|\sigma_{\text{NICS}}| > 1 \text{ ppm}$  or  $|\sigma_{\text{tot}}| > 1 \text{ ppm}$  are presented in the table (see full listing in Table S1 of the supplementary material).

<sup>b</sup> $r_{\text{H}\cdots\text{O}}(\text{\AA})$  is the shortest H to O distance, which is less than  $3 \text{ \AA}$ .

TABLE V. GIPAW calculated  $^1\text{H}$  magnetic shielding (in ppm) for IND (**5**) as part of a IND-NIC co-crystal **5:6**.<sup>a</sup>

	Group	Label	$\sigma_{\text{dia}}^{\text{loc}}$	$\sigma_{\text{lr}}$	$\sigma_{\text{tot}}$	$\sigma_{\text{NICS}}$	$r_{\text{H}\cdots\text{O}}(\text{\AA})^b$
Isolated molecule	CH	2	9.32	14.90	24.22		
	CH <sub>3</sub>	5	9.26	19.57	28.83		
	CH <sub>3</sub>	6	9.23	20.12	29.36		
	H <sub>3</sub> CO	7	9.36	17.98	27.34		
	OH	12	7.09	14.81	21.90		
	CH	13	9.22	14.02	23.24		
	CH	14	9.21	14.39	23.60		
	CH	15	9.24	14.55	23.79		
Full crystal	CH	16	9.25	14.59	23.85		
	CH	2	9.29	15.60	24.89		
	CH <sub>3</sub>	5	9.19	20.30	29.49		
	CH <sub>3</sub>	6	9.28	22.06	31.33		
	H <sub>3</sub> CO	7	9.33	20.37	29.70		
	OH	12	6.88	4.63	11.51		
	CH	13	9.22	16.26	25.48		
	CH	14	9.07	14.5	23.56		
$\Delta\sigma$	CH	15	9.24	15.71	24.96		
	CH	16	9.26	15.38	24.64		
	CH	2	-0.03	0.70	0.67	1.17	...
	CH <sub>3</sub>	5	-0.07	0.73	0.66	1.45	2.50
	CH <sub>3</sub>	6	0.04	1.94	1.98	1.68	...
	H <sub>3</sub> CO	7	-0.02	2.39	2.36	2.54	...
	OH	12	-0.21	-10.18	-10.39	1.56	...
	CH	13	0.00	2.24	2.23	2.52	...
$\Delta\sigma$	CH	14	-0.14	0.10	-0.04	1.57	2.22
	CH	15	0.01	1.16	1.17	1.49	...
	CH	16	0.01	0.79	0.80	1.14	...

<sup>a</sup>Only protons with either  $|\sigma_{\text{NICS}}| > 1 \text{ ppm}$  or  $|\sigma_{\text{tot}}| > 1 \text{ ppm}$  are presented in the table (see full listing in Table S4 of the supplementary material).

<sup>b</sup> $r_{\text{H}\cdots\text{O}}(\text{\AA})$  is the shortest H to O distance, which is less than  $3 \text{ \AA}$ .

TABLE VI. GIPAW calculated  $^1\text{H}$  magnetic shielding (in ppm) for NIC (6) as part of an IND-NIC co-crystal 5:6.<sup>a</sup>

	Group	Label	$\sigma_{dia}^{loc}$	$\sigma^{lr}$	$\sigma_{tot}$	$\sigma_{NICS}$	$r_{\text{H}\cdots\text{O}}(\text{\AA})^b$
Isolated molecule	CH	17	9.37	12.65	22.01		
	CH	18	9.34	12.94	22.27		
	CH	19	9.26	14.46	23.73		
	NH <sub>2</sub>	21	8.77	15.28	24.05		
	NH <sub>2</sub>	22	8.76	15.98	24.74		
Full crystal	CH	17	9.15	11.79	20.94		
	CH	18	9.24	11.51	20.74		
	CH	19	9.15	12.95	22.1		
	NH <sub>2</sub>	21	8.46	11.75	20.21		
	NH <sub>2</sub>	22	8.57	13.67	22.23		
$\Delta\sigma$	CH	17	-0.22	-0.86	-1.07	0.02	2.25
	CH	18	-0.10	-1.43	-1.53	-1.30	2.64
	CH	19	-0.11	-1.51	-1.62	-0.64	2.56
	NH <sub>2</sub>	21	-0.31	-3.53	-3.84	-0.10	2.01
	NH <sub>2</sub>	22	-0.19	-2.32	-2.51	0.14	1.83

<sup>a</sup>Only protons with either  $|\sigma_{NICS}| > 1$  ppm or  $|\sigma_{tot}| > 1$  ppm are presented in the table (see full listing in Table S7 of the supplementary material).

<sup>b</sup> $r_{\text{H}\cdots\text{O}}(\text{\AA})$  is the shortest H to O distance, which is less than 3 Å.

MSCF  $G_R(r)$ , from Eq. (8), for this OH (H1) proton in  $\gamma$ -IND (4), where there is a carboxylic acid hydrogen-bonded dimer. First, in part (a), we show the contributions to the  $^1\text{H}$  shielding for the full crystal (calculation  $I_{\text{fullcell}}$  in Fig. 1). In (b), we show the contribution for the isolated molecule (calculation  $III_{\text{onemol}}$  in Fig. 1). Third, in (c), we show the contribution from the neighbouring NIC molecule to the shielding at the OH site (calculation  $II_{\text{nomol}}$  in Fig. 1). This contribution represents the value of the NICS. The superposition of the preceding two contributions ( $II_{\text{nomol}} + III_{\text{onemol}}$ ) is shown in (d) and represents a “frozen” interaction between the two molecules, in which the charge density around OH is not allowed to adjust to the presence of the neighbouring carboxylate group. Finally, by plotting the difference between this “frozen” contribution [shown in (d)] and the contribution from the full crystal [shown in (a)], i.e.,  $I_{\text{fullcell}} - (II_{\text{nomol}} + III_{\text{onemol}})$ , we obtain a picture

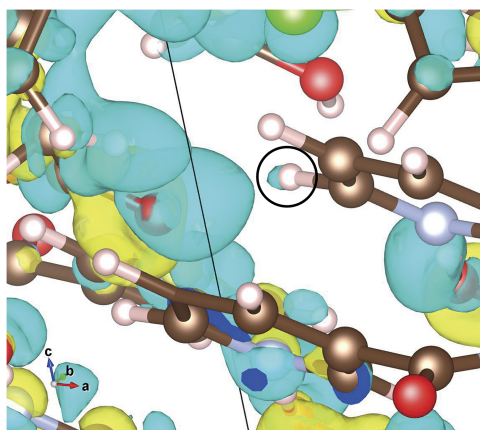


FIG. 4. Magnetic Shielding Contribution Field (MSCF) for site H18 in NIC (6) as part of an IND-NIC co-crystal 5:6 as obtained from the  $II_{\text{nomol}}$  calculation (see Fig. 1). Yellow elements increase the NICS value and blue elements decrease the  $\sigma_{NICS}$  value.

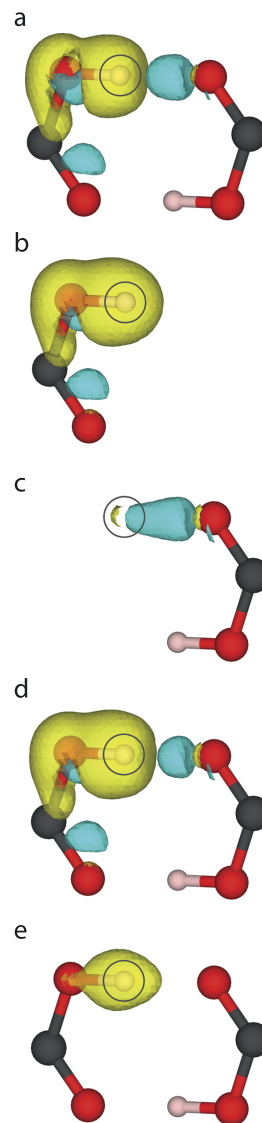


FIG. 5. Using the MSCF to demonstrate the effect of a hydrogen bond on the magnetic shielding of the OH (1) proton in  $\gamma$ -IND (4) (marked with a circle). The magnitude and sign of  $G_R$  [Eq. (8)] are plotted as an isosurface containing volume elements that contribute 0.003 15 ppm or more to the shielding at hydrogen (element volume  $0.0016 \text{\AA}^3$ ). Yellow elements are positive contributions and blue elements are negative contributions. (a) A full crystallographic unit cell calculation (calculation  $I_{\text{fullcell}}$  in Fig. 1). (b) A single molecule calculation (calculation  $III_{\text{onemol}}$  in Fig. 1). (c) An absent molecule calculation (calculation  $II_{\text{nomol}}$  in Fig. 1). (d) The sum of the single molecule and absent molecule ( $III_{\text{onemol}} + II_{\text{nomol}}$ ). (e) A full crystallographic unit cell calculation is subtracted from the sum of the single and absent molecule calculations ( $III_{\text{onemol}} + II_{\text{nomol}} - I_{\text{fullcrs}}$ ). This represents the change in the magnetic shielding of the proton due to the presence of the hydrogen bond.

in (e) of the contribution to the OH proton shielding arising from the change in charge density due to the presence of the hydrogen bond. In other words, (e) is a visual representation of the location of the  $-7.18$  ppm difference between  $\Delta\sigma^{lr}$  ( $-6.83$  ppm) and  $\sigma_{NICS}$  ( $+0.35$  ppm). We see that the change in the induced field at the proton comes from regions close to the nucleus polarized by the oxygen lone pair.

#### IV. CONCLUSIONS

In summary, we have outlined a methodology to quantify the importance of both short-range and long-range



contributions to the magnetic shielding of atoms in molecular crystals. For 2nd period atoms, such as C, changes to the magnetic shielding between a molecule and a crystal can be due to both local changes in the electronic structure and the effects of current at longer distances, e.g., ring currents. The ability to separate these effects assists with the interpretation of the observed chemical shifts. For the special case of protons, the long-range effects dominate over any short-range effects. We have shown how the MSCF provides a visual map of the location of the current contributing to the shielding of a specific atom. In this way, the effects of ring currents can be separated from hydrogen bond donors. In the case of hydrogen-bonded atoms, we see a contribution to the shielding from currents around the donor oxygen atom. For strongly hydrogen bonded atoms, the dominant change in the shielding arises from the polarization of the charge density around the hydrogen bonded proton.

These observations and the tools to visualize the long-range contributions have a clear relevance to the study of NMR crystallography—as the sensitivity of the chemical shift, particularly that for protons, is central to the ability of NMR to distinguish between packing motifs.<sup>37,38</sup> However, this work is also of use in developing new predictive techniques—for example, the use of machine learning techniques to predict NMR chemical shifts. A machine learning approach for the prediction of Si and O shifts has recently been demonstrated.<sup>39</sup> Such an approach should work well for these elements because, as we have shown, the dominant contribution to the current will be local. However, we have shown that for such an approach to be accurate for light atoms, such as H, in a molecular crystal, it is essential to account for long-range effects. The same is true for fragment-based approaches<sup>40</sup> to predict chemical shifts which will need careful validation for the prediction of proton chemical shifts.

## SUPPLEMENTARY MATERIAL

See [supplementary material](#) for the derivation of the long- and short-range decomposition of the current; tables of the magnetic shielding contributions for all nuclei in the  $\gamma$  polymorph of indomethacin, the co-crystal of indomethacin and nicotinamide, and uracil; figures of the positive and negative contributions to the magnetic shielding contribution fields in 1,4-dicyanobenzene; magres files for all compounds studied in this work containing the crystal structure and full shielding tensors.

## ACKNOWLEDGMENTS

This work was supported by the Collaborative Computational Project for NMR Crystallography funded by the EPSRC (UK) Grant Nos. EP/J010510/1 and EP/M022501/1. M.Z. acknowledges funding from the European Union under a Marie Curie Initial Training Network FP7-PEOPLE-2012-ITN Grant Agreement No. 316630 CAS-IDP. This work used the ARCHER UK National Supercomputing Service (<http://www.archer.ac.uk>), for which access was obtained via the UKCP consortium and funded by EPSRC Grant Ref. EP/K013564/1.

- <sup>1</sup>F. Taulelle, *Solid State Sci.* **6**, 1053 (2004).
- <sup>2</sup>R. K. Harris, *Solid State Sci.* **6**, 1025 (2004).
- <sup>3</sup>T. Helgaker, M. Jaszunski, and K. Ruud, *Chem. Rev.* **99**, 293 (1999).
- <sup>4</sup>T. Charpentier, *Solid State Nucl. Magn. Reson.* **40**, 1 (2011).
- <sup>5</sup>C. Bonhomme, C. Gervais, F. Babonneau, C. Coelho, F. Pourpoint, T. Azaïs, S. E. Ashbrook, J. M. Griffin, J. R. Yates, F. Mauri, and C. J. Pickard, *Chem. Rev.* **112**, 5733 (2012).
- <sup>6</sup>A. Hofstetter and L. Emsley, *J. Am. Chem. Soc.* **139**, 2573 (2017).
- <sup>7</sup>D. Dudenko, A. Kiersnowski, J. Shu, W. Pisula, D. Sebastiani, H. W. Spiess, and M. R. Hansen, *Angew. Chem., Int. Ed.* **51**, 11068 (2012).
- <sup>8</sup>J. R. Yates, T. N. Pham, C. J. Pickard, F. Mauri, A. M. Amado, A. M. Gil, and S. P. Brown, *J. Am. Chem. Soc.* **127**, 10216 (2005).
- <sup>9</sup>J. Schmidt, A. Hoffmann, H. W. Spiess, and D. Sebastiani, *J. Phys. Chem. B* **110**, 23204 (2006).
- <sup>10</sup>A.-C. Uldry, J. M. Griffin, J. R. Yates, M. Pérez-Torrallba, M. D. S. María, A. L. Webber, M. L. L. Beaumont, A. Samoson, R. M. Claramunt, C. J. Pickard, and S. P. Brown, *J. Am. Chem. Soc.* **130**, 945 (2008).
- <sup>11</sup>L. Mafra, S. M. Santos, R. Siegel, I. Alves, F. A. Almeida Paz, D. Dudenko, and H. W. Spiess, *J. Am. Chem. Soc.* **134**, 71 (2012).
- <sup>12</sup>P. v. R. Schleyer, C. Maerker, A. Dransfeld, H. Jiao, and N. J. R. v. E. Hommes, *J. Am. Chem. Soc.* **118**, 6317 (1996).
- <sup>13</sup>Z. Chen, C. S. Wannere, C. Corminboeuf, R. Puchta, and P. v. R. Schleyer, *Chem. Rev.* **105**, 3842 (2005).
- <sup>14</sup>J. C. Facelli, *Magn. Reson. Chem.* **44**, 401 (2006).
- <sup>15</sup>D. Sebastiani and K. N. Kudin, *ACS Nano* **2**, 661 (2008).
- <sup>16</sup>D. Sebastiani, *ChemPhysChem* **7**, 164 (2006).
- <sup>17</sup>M. Kibalchenko, M. C. Payne, and J. R. Yates, *ACS Nano* **5**, 537 (2011).
- <sup>18</sup>C. J. Pickard and F. Mauri, *Phys. Rev. B* **63**, 245101 (2001).
- <sup>19</sup>K. Kobayashi and M. Tsukada, *Phys. Rev. B* **38**, 8566 (1988).
- <sup>20</sup>F. Mauri, B. G. Pfommer, and S. G. Louie, *Phys. Rev. Lett.* **77**, 5300 (1996).
- <sup>21</sup>M. Profeta, M. Benoit, F. Mauri, and C. J. Pickard, *J. Am. Chem. Soc.* **126**, 12628 (2004).
- <sup>22</sup>T. Gregor, F. Mauri, and R. Car, *J. Chem. Phys.* **111**, 1815 (1999).
- <sup>23</sup>P. Florian, E. Veron, T. F. G. Green, J. R. Yates, and D. Massiot, *Chem. Mater.* **24**, 4068 (2012).
- <sup>24</sup>J. C. Johnston, R. J. Iulucci, J. C. Facelli, G. Fitzgerald, and K. T. Mueller, *J. Chem. Phys.* **131**, 144503 (2009).
- <sup>25</sup>M. Woźnińska, S. Grabowsky, P. M. Dominiak, K. Woźniak, and D. Jayatilaka, *Sci. Adv.* **2**, e1600192 (2016).
- <sup>26</sup>C. H. Görbitz, *Crystallogr. Rev.* **21**, 160 (2015).
- <sup>27</sup>S. P. Brown, T. Schaller, U. P. Seelbach, F. Koziol, C. Ochsenfeld, F. G. Klärner, and H. W. Spiess, *Angew. Chem., Int. Ed.* **40**, 717 (2001).
- <sup>28</sup>C. Ochsenfeld, F. Koziol, S. P. Brown, T. Schaller, U. P. Seelbach, and F.-G. Klärner, *Solid State Nucl. Magn. Reson.* **22**, 128 (2002).
- <sup>29</sup>J. P. Bradley, S. P. Velaga, O. N. Antzutkin, and S. P. Brown, *Cryst. Growth Des.* **11**, 3463 (2011).
- <sup>30</sup>D. V. Dudenko, J. R. Yates, K. D. M. Harris, and S. P. Brown, *CrystEngComm* **15**, 8797 (2013).
- <sup>31</sup>S. J. Clark, M. D. Segall, C. J. Pickard, P. J. Hasnip, M. I. J. Probert, K. Refson, and M. C. Payne, *Z. Kristallogr. - Cryst. Mater.* **220**, 567 (2005).
- <sup>32</sup>K. Lejaeghere, G. Bihlmayer, T. Björkman, P. Blaha, S. Blügel, V. Blum, D. Caliste, I. E. Castelli, S. J. Clark, A. Dal Corso, S. de Gironcoli, T. Deutsch, J. K. Dewhurst, I. Di Marco, C. Draxl, M. Duaak, O. Eriksson, J. A. Flores-Livas, K. F. Garrity, L. Genovese, P. Giannozzi, M. Giantomassi, S. Goedecker, X. Gonze, O. Grånäs, E. K. U. Gross, A. Gulans, F. Gygi, D. R. Hamann, P. J. Hasnip, N. A. W. Holzwarth, D. Iuan, D. B. Jochym, F. Jollet, D. Jones, G. Kresse, K. Koepnik, E. Küçükbenli, Y. O. Kvashnin, I. L. M. Loch, S. Lubeck, M. Marsman, N. Marzari, U. Nitzsche, L. Nordström, T. Ozaki, L. Paulatto, C. J. Pickard, W. Poelmans, M. I. J. Probert, K. Refson, M. Richter, G.-M. Rignanese, S. Saha, M. Scheffler, M. Schlipf, K. Schwarz, S. Sharma, F. Tavazza, P. Thunström, A. Tkatchenko, M. Torrent, D. Vanderbilt, M. J. van Setten, V. Van Speybroeck, J. M. Wills, J. R. Yates, G.-X. Zhang, and S. Cottenier, *Science* **351**, aad3000 (2016).
- <sup>33</sup>H. J. Monkhorst and J. D. Pack, *Phys. Rev. B* **13**, 5188 (1976).
- <sup>34</sup>J. P. Perdew, K. Burke, and M. Ernzerhof, *Phys. Rev. Lett.* **77**, 3865 (1996).
- <sup>35</sup>A. Tkatchenko and M. Scheffler, *Phys. Rev. Lett.* **102**, 073005 (2009).
- <sup>36</sup>J. R. Yates, C. J. Pickard, and F. Mauri, *Phys. Rev. B* **76**, 024401 (2007).
- <sup>37</sup>E. Salager, G. M. Day, R. S. Stein, C. J. Pickard, B. Elena, and L. Emsley, *J. Am. Chem. Soc.* **132**, 2564 (2010).
- <sup>38</sup>S. P. Brown, *Solid State Nucl. Magn. Reson.* **41**, 1 (2012).
- <sup>39</sup>J. Cuny, Y. Xie, C. J. Pickard, and A. A. Hassanali, *J. Chem. Theory Comput.* **12**, 765 (2016).
- <sup>40</sup>G. J. Beran, *Chem. Rev.* **116**, 5567 (2016).